Minority carriers in graphite and the H-point magnetoreflection spectra*

W. W. Toy† and M. S. Dresselhaus†

Department of Electrical Engineering and Computer Science and the Center for Materials Science and Engineering, Massachusetts Institute of Technology, Cambridge, Massachusetts 02139

G. Dresselhaus

Francis Bitter National Magnet Laboratory,‡ Massachusetts Institute of Technology, Cambridge, Massachusetts 02139 and Lincoln Laboratory, Massachusetts Institute of Technology, Lexington, Massachusetts 02173

(Received 30 August 1976)

Analysis of the H-point magnetoreflection spectra of graphite is shown to be sensitive not only to the magnitude, but also to the *sign* of the Slonczewski-Weiss-McClure band parameter Δ. The demonstration that Δ is small and negative provides a definite assignment for the larger of the minority de Haas–van Alphen periods to the Brillouin-zone corner, the H-point. This assignment is in good agreement with other experimental data.

I. INTRODUCTION

The search for an interpretation for the two experimentally observed minority de Haas–van Alphen periods represents one of the major unresolved problems in the electronic-energy-band structure of graphite.[1-7] In this paper, it is shown that the negative sign of the Slonczewski-Weiss-McClure band parameter Δ, determined from analysis of H-point magnetoreflection data, in conjunction with these minority de Haas–van Alphen periods leads to a definitive assignment for one of the minority de Haas–van Alphen periods.

The first observation of a minority de Haas–van Alphen (dHvA) period was reported by Soule in 1964 for single-crystal graphite.[1] His result of $P_1 = (1.35 \pm 0.3) \times 10^{-4}\ \mathrm{G}^{-1}$ was soon confirmed by the observations of Williamson *et al.*[2] who reported a period of $P_1 = (1.35 \pm 0.1) \times 10^{-4}\ \mathrm{G}^{-1}$. In their dHvA study, Williamson *et al.* also reported a period of $P_2 = (3.03 \pm 0.15) \times 10^{-4}\ \mathrm{G}^{-1}$ in pyrolytic graphite.[2,8] By studying the quantum oscillations of the Hall conductivity σ_{xy}, Woollam was able to identify the period P_1 as characteristic of a minority-hole pocket.[9]

Soon after the discovery of minority dHvA periods, it was proposed[2,10] that a minority period could be associated with an extremal Fermi cross-sectional area about the H point on the Brillouin-zone boundary. According to this interpretation, the minority surface shown in Fig. 1 results from the translation by a reciprocal-lattice vector of the cap portion of the Fermi surface which protrudes beyond the Brillouin-zone boundary (see Fig. 1).

At first it was thought that there was only one kind of minority dHvA period and that it had different values for single-crystal as compared with pyrolytic graphite.[2] More detailed studies later showed that the two minority periods both occur in single-crystal and in pyrolytic graphite.[3,6] Although the model shown in Fig. 1 predicts two minority periods when spin-orbit interaction is introduced,[2,10] the magnitude of the spin-orbit interaction is very small (<1 meV)[11,12] and can account for a difference of no more than $\approx 10\%$ between two spin-orbit split minority periods.

The Fermi-surface extremal cross-sectional area about the H point in Fig. 1 can be calculated from the Slonczewski-Weiss-McClure (SWMcC) model to yield a minority H-point dHvA period of[2,10]

$$P_H = (3e/2\hbar c)\, a_0^2 \gamma_0^2 / E_F (E_F - \Delta)\,, \tag{1}$$

in which the lattice constant $a_0 = 2.46$ Å. A value of $\gamma_0 = 3.1$ eV is obtained for the largest of the graphite band parameters (corresponding to the nearest-neighbor interaction energy) from H-point magnetoreflection data[13] and from a recent analysis of diamagnetic susceptibility data, including the effects of trigonal warping.[14] The Fermi energy E_F is determined by the semimetallic requirement of hole and electron carrier compensation and by the magnitude of the observed *majority* electron and hole dHvA periods, and is therefore set at $E_F = -0.025$ eV with an estimated error $\sim \pm 5\%$. With the values for γ_0 and E_F fixed, it is possible to achieve agreement with either of the minority-carrier periods P_1 or P_2 depending on the choice of the *sign* and magnitude for Δ. With the choice of the negative sign, a fit to P_2 is achieved for $\Delta = -0.006$ eV, while the positive sign provides a fit to the other period P_1 for $\Delta = +0.017$ eV.

Previous studies of these minority periods have not conclusively identified either P_1 or P_2 with P_H.[6,12] Woollam[6] has suggested that both periods are associated with the Fermi surface near the

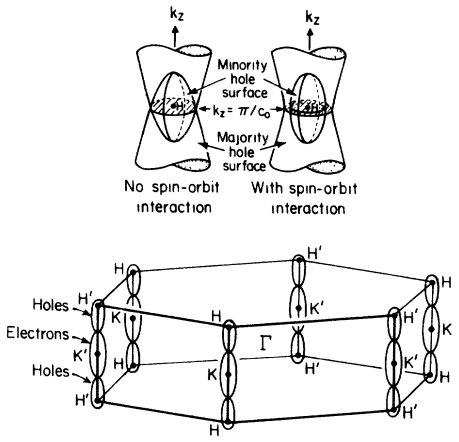

FIG. 1. Fermi surface for minority hole pocket near the Brillouin-zone corner (the H point) shown in the extended-zone scheme. This pocket is formed by the overlap of the portions of the Fermi surface which extend beyond the Brillouin-zone boundary and is illustrated for no-spin-orbit interaction, and including spin-orbit interaction. The extremal cross section around the H point and perpendicular to the c axis is indicated. Bottom: Hexagonal Brillouin zone for graphite showing schematically the locations of the hole and electron Fermi surfaces. Of particular interest are the portions of the hole surface which project beyond the Brillouin-zone boundary and give rise to the minority surface shown in the top figure.

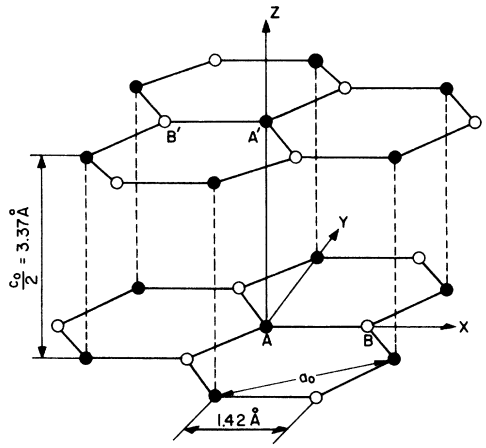

FIG. 2. Graphite crystal structure showing the stacking arrangement and the resulting difference between A atoms (which have neighboring atoms A' immediately above and below) and B atoms (which do not, but rather have displaced B' atoms in adjacent layer planes). The difference in potential energy between the A and B sites is expressed by the SWMcC band parameter Δ. The lattice constant a_0 is the distance between nearest-neighbor A atoms (or B atoms) in the layer plane and the lattice constant $\frac{1}{2}c_0$ is the distance between layer planes.

H point, while Spain[12] has proposed that one of the periods may possibly be associated with the small cross sections which are present in the region where the electron and hole Fermi surfaces make contact (the so-called legs or feet).

The following arguments have been proposed to favor the identification of P_H with P_2. A somewhat better fit is achieved with previously reported H-point magnetoreflection results.[13] In the absence of an H-point magnetoreflection line-shape calculation, there has been some doubt about the interpretation of the resonant magnetic fields within the resonance linewidths. For this reason, it has not been possible in the past to distinguish conclusively between the two possible identifications for P_H on the basis of magnetoreflection data. The interpretation of the diamagnetic susceptibility data also favors the identification of P_2 with P_{11}.[14] Since the analysis of diamagnetic susceptibility data is also sensitive to the values of other parameters (e.g., γ_0 and γ_3), the determination of Δ cannot be made independently.

We show in the present work that the H-point magnetoreflection data do in the limit of low quantum number provide strong evidence for a negative sign for Δ, which arises from the difference in potential energy at the inequivalent A and B lattice sites (see Fig. 2). This work consequently yields a definitive identification of the minority period P_2 with P_H at the Brillouin-zone boundary (Fig. 1).

In Sec. II, application of SWMcC band model is made to the energy levels, wave functions, and selection rules for H-point interband Landau-level transitions; the transitions that are sensitive to the sign of Δ are emphasized. In Sec. III, results for H-point magnetoreflection transitions are presented and discussed, with particular reference to the lowest-quantum-number transitions which provide strong evidence in support of the negative sign for Δ and an identification of the minority dHvA period P_2 with P_H. The paper concludes with Sec. IV which discusses other experimental evidence in support of the identification of P_2 with P_H.

II. INTERBAND TRANSITIONS AT THE H POINT

The SWMcC Hamiltonian for the four π bands in graphite is described by a (4×4) Hamiltonian which has been discussed extensively in the literature.[7] The effective Hamiltonian in the presence of a magnetic field H along the c axis has been developed by McClure[15] and others.[16,17] In the approximation that $\gamma_3 = 0$, this effective magnetic Hamiltonian for a state N can be written

$$\mathcal{H}(\xi,N)=\begin{bmatrix} \epsilon_1 & 0 & -(\tfrac{1}{2}B)^{1/2}(1-\nu)N^{1/2} & -(\tfrac{1}{2}B)^{1/2}(1-\nu)(N+1)^{1/2} \\ 0 & \epsilon_2 & (\tfrac{1}{2}B)^{1/2}(1+\nu)N^{1/2} & -(\tfrac{1}{2}B)^{1/2}(1+\nu)(N+1)^{1/2} \\ -(\tfrac{1}{2}B)^{1/2}(1-\nu)N^{1/2} & (\tfrac{1}{2}B)^{1/2}(1+\nu)N^{1/2} & \epsilon_3 & 0 \\ -(\tfrac{1}{2}B)^{1/2}(1-\nu)(N+1)^{1/2} & -(\tfrac{1}{2}B)^{1/2}(1+\nu)(N+1)^{1/2} & 0 & \epsilon_3 \end{bmatrix}, \tag{2}$$

where the various quantities in Eq. (2) are given by

$$\epsilon_1=\Delta+\gamma_1\Gamma+\tfrac{1}{2}\gamma_5\Gamma^2,\quad \epsilon_2=\Delta-\gamma_1\Gamma+\tfrac{1}{2}\gamma_5\Gamma^2,\quad \epsilon_3=\tfrac{1}{2}\gamma_2\Gamma^2,\quad B=\gamma_0^2(\tfrac{3}{2}a_0^2)eH/\hbar c,\quad \nu=(\gamma_4/\gamma_0)\Gamma,\quad \Gamma=2\cos(\pi\xi). \tag{3}$$

Even at the highest magnetic fields (150 kG) used in the magnetoreflection experiments, the paramagnetic terms in $\mu_B H$ (μ_B is the Bohr magneton) are very small compared with other pertinent energies, and are for this reason neglected in writing the magnetic Hamiltonian [Eq. (2)]. The effective-mass wave functions used to derive Eq. (2) are written

$$\psi(N)=\begin{cases}(C_1^N\phi_N,\ C_2^N\phi_N,\ C_{31}^N\phi_{N-1},\ C_{32}^N\phi_{N+1}); & N\geq 1,\\ (C_1^0\phi_0,\ C_2^0\phi_0,\ 0,\ C_{32}^0\phi_1); & N=0,\\ (0,\ 0,\ 0,\ C_{32}^{-1}\phi_0); & N=-1,\end{cases} \tag{4}$$

where the ϕ_N denote harmonic-oscillator-type effective-mass functions associated with the four π-band wave functions located at the Brillouin-zone edge. The coefficients C are constants which express the magnitude of the various harmonic oscillator states contained in a particular eigenvector of the magnetic Hamiltonian. The solutions of the magnetic eigenvalue problem, Eq. (2), lead to a set of four Landau ladders, in which the levels are labeled by the index N. The ξ dependence of these ladders is illustrated in the Landau-level contour diagram given in Fig. 3. This figure is constructed for $\Delta<0$, in accordance with the findings of the present study, but in contrast with previously published Landau-level contour diagrams.[18] In Fig. 3 we have also taken $\gamma_3=0$ for simplicity because neither the energy levels nor the optical matrix elements near the H point depend on γ_3.

We will now use these Landau levels to interpret the magnetoreflection spectra. The magnetoreflection resonances emphasize contributions from regions in the Brillouin zone where there is a singularity in the joint density of states connecting the Landau levels involved in the transition. From Fig. 3 it is seen that both points K and H satisfy the resonant condition. In this paper, we will be concerned with Landau-level transitions about the H point, which we refer to as H-point transitions.

In Fig. 3, we have labeled the magnetic energy levels at the H point in accordance with the notation given above. The level crossing which occurs between the levels labeled $N=0$ and $N=-1$ in Fig. 3 is a simple level crossing; i.e., there is no interaction between the levels as they cross. For interaction to occur, these levels must differ in quantum number by $\Delta N=\pm 3n, n=1,2,3,\ldots$. This result has the significance that the H-point energy level and wave function designations are given by the same formulas, independent of the sign of Δ and independent of the ordering for the two lowest quantum-number levels at the

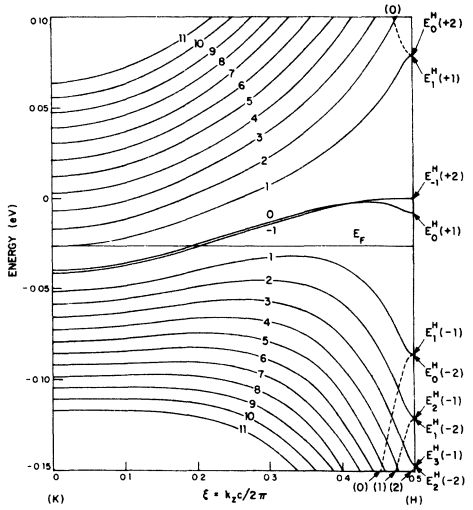

FIG. 3. Magnetic energy levels labeled by N along the HKH axis for $H=50$ kG and $\gamma_3=0$. The levels at the H point are labeled by both a Landau-level quantum number and ladder index. The crossing of the $E_0^H(+1)$ and $E_{-1}^H(+2)$ levels is a consequence of the negative sign of Δ. The magnetic energy levels of the E_1 and E_2 bands are shown as dashed curves, and away from the H point are labeled by (N). The band parameters used to construct this figure are approximately those in sets C and J in Ref. 26 with $\gamma_0=3.16$ eV and $\Delta=-0.008$ eV.

H point.

Since the magnetic energy levels at the H point in the Brillouin zone depend only on the two band parameters γ_0 and Δ, the study of H-point interband Landau-level transitions can be utilized to evaluate these parameters independently and accurately. At the H point we have $\xi = \frac{1}{2}$, $\Gamma = 0$, and the magnetic Hamiltonian is independent of γ_3. Thus the Hamiltonian in Eq. (2) can be decoupled to yield the four H-point eigenvalues with $N \geq 1$,

$$E_N^H(\pm 1) = \tfrac{1}{2}\Delta \pm \tfrac{1}{2}(\Delta^2 + 4NB)^{1/2}, \qquad E_N^H(\pm 2) = \tfrac{1}{2}\Delta \pm \tfrac{1}{2}[\Delta^2 + 4(N+1)B]^{1/2}. \tag{5}$$

In Eq. (5) we have used the superscript index H to denote the H point in the Brillouin zone, the subscript N to refer to the quantum index in Eq. (2) and the arguments ± 1 and ± 2 to classify the Landau-level ladders, with $+2$ being the highest in energy, followed by $+1$, -1, and -2 in that order. We note the degeneracy of levels in the ± 1 ladders with levels in the ± 2 ladders at the H point: $E_{N+1}^H(\pm 1) = E_N^H(\pm 2)$ for $N \geq 1$.

The eigenfunctions associated with these eigenvalues are

$$\Phi_N^H(\pm 1) = (0,\ C_{11}^{\pm 1,N}\phi_N,\ C_{31}^{\pm 1,N}\phi_{N-1},\ 0) \tag{6a}$$

$$\Phi_N^H(\pm 2) = (C_{12}^{\pm 2,N}\phi_N,\ 0,\ 0,\ C_{32}^{\pm 2,N}\phi_{N+1}). \tag{6b}$$

in which the coefficients $C_{11}^{\pm 1,N}$ and $C_{12}^{\pm 2,N}$ are related to C_1^N and C_2^N in Eq. (4) by

$$C_{11}^{\pm 1,N} = (C_1^N - C_2^N)/\sqrt{2}, \qquad C_{12}^{\pm 2,N} = (C_1^N + C_2^N)/\sqrt{2}. \tag{7}$$

In the limit $|\Delta| \ll (BN)^{1/2}$, which is generally satisfied for magnetic fields at which interband Landau-level transitions are observed (except for the very lowest quantum-number levels)

$$C_{12}^{\pm 2,N} \simeq 1/\sqrt{2},\quad C_{32}^{\pm 2,N} \simeq \mp 1, \tag{8}$$

and the level degeneracy at the H point implies that

$$C_{31}^{\pm 1,N+1} \simeq C_{32}^{\pm 2,N},\quad C_{11}^{\pm 1,N+1} \simeq C_{12}^{\pm 2,N}. \tag{9}$$

To find the selection rules for intraband and interband Landau-level transitions, we consider matrix elments of the optical-perturbation Hamiltonian[10]

$$\mathcal{H}'_{\rm op} = -(e/\hbar c)(A^+\mathfrak{D}_{\rm op}^- + A^-\mathfrak{D}_{\rm op}^+), \tag{10}$$

where $A^\pm$ denotes the vector potential for right and left circular polarization, and the matrices $\mathfrak{D}_{\rm op}^\pm$ are defined explicitly in Ref. 10. These matrix elements are expressed in the same representation as was used to bring the magnetic Hamiltonian [Eq. (2)] into block form at the H point. This unitary transformation also brings $\mathcal{H}'_{\rm op}$ (or $\mathfrak{D}_{\rm op}^-$ and $\mathfrak{D}_{\rm op}^+$) into block form. Writing $\tilde{\mathfrak{D}}_{\rm op}^\pm = U\mathfrak{D}_{\rm op}^\pm U^{-1}$, we denote the (2×2) blocks by

$$\tilde{\mathfrak{D}}_{{\rm op},1}^- = \begin{pmatrix} (\hbar^2/2m)\kappa_- & \sqrt{2}\,\pi_{13}^H \\ 0 & (\hbar^2/2m)\kappa_- \end{pmatrix} \tag{11a}$$

and

$$\tilde{\mathfrak{D}}_{{\rm op},2}^- = \begin{pmatrix} (\hbar^2/2m)\kappa_- & 0 \\ \sqrt{2}\,\pi_{13}^H & (\hbar^2/2m)\kappa_- \end{pmatrix}, \tag{11b}$$

in which the Landau-level ladder index is included in $\tilde{\mathfrak{D}}_{\rm op}^-$ as a subscript (1 for ± 1 ladders and 2 for ± 2 ladders). The $\vec{k}\cdot\vec{p}$ parameter π_{13}^H is related to the SWMcC parameters by

$$\pi_{13}^H = -3a_0\gamma_0/2\sqrt{6}\ . \tag{11c}$$

The nonvanishing matrix elements for Landau-level transitions correspond to the $\Delta N = \pm 1$ selection rule and are given by

$$(\Phi_{N-1}^H(\pm 1)\,|\,\tilde{\mathfrak{D}}_{{\rm op},1}^-\,|\,\Phi_N^H(\pm 1)) = \sqrt{2}\,\pi_{13}^H C_{11}^{\pm 1,N-1*} C_{31}^{\pm 1,N} \tag{12a}$$

and

$$(\Phi_{N-1}^H(\pm 2)\,|\,\tilde{\mathfrak{D}}_{{\rm op},2}^-\,|\,\Phi_N^H(\pm 2)) = \sqrt{2}\,\pi_{13}^H C_{12}^{\pm 2,N} C_{32}^{\pm 2,N-1*}, \tag{12b}$$

in which only the nonzero components of the eigenfunctions $\Phi_N^H(\pm 1)$ and $\Phi_N^H(\pm 2)$ in Eq. (6) are employed in calculating the indicated matrix elements. Application of the approximations in Eqs. (8) and (9) yields

$$(\Phi_{N-1}^H(\pm 1)\,|\,\tilde{\mathfrak{D}}_{{\rm op},1}^-\,|\,\Phi_N^H(\pm 1)) \simeq (\Phi_{N-1}^H(\pm 2)\,|\,\tilde{\mathfrak{D}}_{{\rm op},2}^-\,|\,\Phi_N^H(\pm 2)) \simeq \pi_{13}^H/\sqrt{2}\,. \tag{13}$$

The nonvanishing matrix elements for the other sense of circular polarization can be found from the relation

$$(\Phi_{n,j}\,|\,\tilde{\mathfrak{D}}_{\rm op}^-\,|\,\Phi_{n',j'}) = (\Phi_{n',j'}\,|\,\tilde{\mathfrak{D}}_{\rm op}^+\,|\,\Phi_{n,j}) \tag{14}$$

in which the (n,n') and (j,j') indices denote Landau-*level* and Landau-*ladder* indices, respectively. In making an actual Landau-level transition, an electron absorbs electromagnetic energy in going from an occupied to an unoccupied state. This restriction yields the selection rules for observable transitions[10] with $N \geq 1$:

$$E_N^H(-2) \to E_{N+1}^H(+2) \quad \text{and} \quad E_N^H(-1) \to E_{N+1}^H(+1), \tag{15a}$$

with $\ominus$ circular polarization, and

$$E_N^H(-1) \to E_{N-1}^H(+1) \quad \text{and} \quad E_N^H(-2) \to E_{N-1}^H(+2), \tag{15b}$$

with $\oplus$ circular polarization, following the notation for circular polarization used in Refs. 18 and 19. Interband Landau-level transitions are ob-

served in a magnetoreflection experiment whenever the photon energy $\hbar\omega$ is equal to the energy difference between any one of the four pairs of coupled magnetic energy levels, subject to the selection rules of Eq. (15). The resulting resonant conditions for $N \geq 1$ on ladders (1) and (2) for both senses of circular polarization are

$$\hbar\omega_N^{(-)} = E_N^H(+2) - E_{N-1}^H(-2) = E_{N+1}^H(+1) - E_N^H(-1), \tag{16a}$$

$$\hbar\omega_N^{(+)} = E_N^H(+1) - E_{N+1}^H(-1) = E_{N-1}^H(+2) - E_N^H(-2), \tag{16b}$$

$$\hbar\omega_N^{(+)} = \hbar\omega_N^{(-)} = \tfrac{1}{2}(\Delta^2 + 4NB)^{1/2} + \tfrac{1}{2}[\Delta^2 + 4(N+1)B]^{1/2}. \tag{16c}$$

At high magnetic fields, the dominant term in Eq. (16) is the term proportional to $B = \gamma_0^2 3a_0^2 eH/2\hbar c$. Since this factor is also proportional to the quantum number N or to $(N+1)$, the H-point magnetoreflection data at high quantum number and high magnetic field are sensitive to a single-band parameter $|\gamma_0|$, and have been used to provide an accurate value for $|\gamma_0|$.[13,20] For lower quantum numbers and lower magnetic fields, the term in Δ^2 becomes important and a value for $|\Delta|$ can be deduced from magnetoreflection data in this limit.[13,20] What is of particular interest is that the transitions discussed in Eq. (16) are sensitive only to the *absolute* values of γ_0 and of Δ.

On the other hand, the Landau-level transitions to the lowest quantum states, $E_0^H(+1)$ and $E_{-1}^H(+2)$ assume a different form and are in fact sensitive to the *sign* of Δ. Therefore we shall give special attention to these transitions in the present work. The levels for $N=0$ are found by applying a similar unitary transformation as is used to bring Eq. (2) into block form. The transformed Hamiltonian for $N=0$ at the H point ($\xi = \frac{1}{2}$) is written

$$\tilde{\mathcal{H}}(\tfrac{1}{2}, 0) = \begin{pmatrix} \Delta & 0 & -\sqrt{B} \\ 0 & \Delta & 0 \\ -\sqrt{B} & 0 & 0 \end{pmatrix}, \tag{17}$$

in which the entries in rows and columns 1 and 3 correspond to the ± 2 Landau ladders, for which the eigenfunctions are given correctly by Eq. (6b) with $N=0$.

The magnetic field dependence of the levels $E_0^H(\pm 2)$ is similar to that of the other levels in the ± 2 ladders and these levels follow the general degeneracy pattern given by Eq. (5),

$$E_0^H(\pm 2) = E_1^H(\pm 1) = \tfrac{1}{2}\Delta \pm \tfrac{1}{2}(\Delta^2 + 4B)^{1/2}. \tag{18}$$

The (2,2) entry in Eq. (17) corresponds to the $+1$ Landau ladder and is a special level with an eigenfunction

$$\Phi_0^H(+1) = (0, \phi_0, 0, 0) \tag{19}$$

and an eigenvalue

$$E_0^H(+1) = \Delta. \tag{20}$$

This level is not degenerate with any other level at the H point and has only a very small magnetic field dependence for $H \lesssim 150$ kG. From Eq. (17) it is seen that there is no state $\Phi_0^H(-1)$, corresponding to the -1 Landau ladder.

Finally, the magnetic Hamiltonian for $N=-1$ is a 1×1 matrix which also gives rise to a special state

$$\Phi_{-1}^H(+2) = (0, 0, 0, \phi_0), \tag{21}$$

with a nondegenerate eigenvalue

$$E_{-1}^H(+2) = 0. \tag{22}$$

For convenience this special state is associated with the $+2$ ladder. From a semiclassical point of view, both the $+2$ and -2 Landau ladders have in common the lowest quantum-number state $\Phi_{-1}^H(+2)$; similarly, the ± 1 Landau ladders have in common $\Phi_0^H(+1)$ as their lowest quantum-number state.

As far as transitions to the $E_0^H(+2)$ Landau level are concerned, the discussion given above for the $N \geq 1$ levels applies equally well. Although the $E_0^H(-2)$ level is similar to other levels in the -2 ladder, transitions from this state can be made to the special level $E_{-1}^H(+2)$ only for the case of $\oplus$ circular polarization [see Eq. (15)]. The optical matrix element for this transition is

$$(\Phi_{-1}^H(+2)\,|\,\tilde{\mathfrak{D}}_{op,2}^-\,|\,\Phi_0^H(-2)) = \sqrt{2}\,\pi_{13}^H C_{12}^{-2,0}. \tag{23}$$

The other special H-point Landau level transition is made to the nondegenerate level $E_0^H(+1)$ and again only occurs for the $\oplus$ circular polarization [see Eq. (15)]. The matrix element in this case is

$$(\Phi_0^H(+1)\,|\,\tilde{\mathfrak{D}}_{op,1}^-\,|\,\Phi_1^H(-1)) = \sqrt{2}\,\pi_{13}^H C_{31}^{-1,1}, \tag{24}$$

and from Eqs. (8) and (9) the approximate relations

$$(\Phi_{-1}^H(+2)\,|\,\tilde{\mathfrak{D}}_{op,2}^-\,|\,\Phi_0^H(-2)) \simeq (\Phi_0^H(+1)\,|\,\tilde{\mathfrak{D}}_{op,1}^-\,|\,\Phi_1^H(-1)) \simeq \pi_{13}^H \tag{25}$$

are obtained showing that the square of the matrix element controlling transitions to the two special levels is approximately twice as large as to the ordinary degenerate H-point levels. The other interesting feature about these special transitions is that they both occur only for the $\oplus$ circular polarization.

Interband transitions to these special levels satisfy the resonant conditions

$$\hbar\omega_{01}^{(+)} = E_0^H(+1) - E_1^H(-1) = [\tfrac{1}{2}\Delta + \tfrac{1}{2}(\Delta^2 + 4B)^{1/2}] , \tag{26a}$$

$$\hbar\omega_{02}^{(+)} = E_{-1}^H(+2) - E_0^H(-2) = [-\tfrac{1}{2}\Delta + \tfrac{1}{2}(\Delta^2 + 4B)^{1/2}] , \tag{26b}$$

in which the subscripts on the frequency ω include both $N=0$ and a ladder index since these transitions are no longer degenerate, as is the case for $N \geq 1$. The presence of the term $\frac{1}{2}\Delta$ outside of the square-root radical in Eqs. (26) leads to a sensitivity to the sign of Δ. Upon reversal of the sign of Δ, the magnitudes of the quantities in square brackets in Eqs. (26a) and (26b) become interchanged. The significance of this result is that to obtain the sign of Δ from an H-point magnetoreflection experiment, not only is it necessary to observe the two transitions to the nondegenerate H-point states, but it is also essential to identify each of these transitions with the appropriate ± 1 or ± 2 ladder. Thus the H-point magnetoreflection *line shape* must be used to assign these magnetoreflection resonances to a particular Landau ladder.

From the above discussion we see that the magnetic energy levels are arranged into two ladders (± 1 and ± 2). Interband Landau level transitions about the H point are made between ladders -1 and $+1$ and between ladders -2 and $+2$. Because of the degeneracy of the H-point levels for $N \geq 1$ we will see that the experimental line shapes for transitions between these degenerate levels will be similar for $\oplus$ and $\ominus$ circular polarization. On the other hand, the line shapes of the transitions to the nondegenerate levels $E_0^H(+1) = \Delta$ and $E_{-1}^H(+2) = 0$ will be different from each other and from the higher quantum-number transitions. We use this difference in line shape to distinguish whether the final state for an observed magnetoreflection resonance is the $E_0^H(+1)$ or $E_{-1}^H(+2)$ level. Then Eqs. (26) can be used to determine the sign of Δ.

In carrying out a magnetoreflection line-shape calculation, it is necessary to find the energy levels and matrix elements not only at the H point as discussed above, but also away from the H point. This information is readily obtained from the full SWMcC magnetic Hamiltonian by expanding the terms in $\mathcal{H}$ and $\mathcal{H}'_{op}$ about the H point ($\xi = \frac{1}{2}$). As we move away from the H point, the magnetic energy levels in ladder -1 increase in energy to join up with the magnetic energy level structure associated with the E_3 valence band (see Fig. 3). In contrast, the magnetic energy levels in the -2 ladder decrease in energy as we move away from the H point and eventually join up with the magnetic energy levels of the E_2 valence band. In a similar way, the magnetic energy levels of the $+1$ ladder join up with the E_3 conduction-band levels while the levels in the $+2$ ladder join up with the E_1 conduction-band levels. The repulsion between the levels in ladders -1 and -2 (and correspondingly in ladders $+1$ and $+2$) arises through the $\gamma_1\Gamma$ and $\gamma_4\Gamma$ terms which are nonvanishing away from the H point.

III. *H*-POINT MAGNETOREFLECTION STUDIES

Magnetoreflection studies of interband Landau-level transitions about the H point in the Brillouin zone were reported as far back as 1965[13,20] in a study directed toward obtaining quantitative values for the parameters which enter the SWMcC band model for graphite.[7] These early studies were carried out with unpolarized light and were interpreted using Eq. (5) so that only the magnitudes of the two SWMcC band parameters γ_0 and Δ were determined, the quoted values[13] being $|\gamma_0| = 3.18 \pm 0.02$ eV and $|\Delta| = 0.009 \pm 0.003$ eV. Magnetoreflection measurements have for convenience been carried out on pyrolytic graphite from which large optical surfaces are easily prepared. There has been some question as to whether the SWMcC band model was applicable to pyrolytic graphite, and if applicable whether the band parameters of the model would be the same for pyrolytic and natural single-crystal graphite. Recent studies on pyrolytic, single-crystal, and kish graphite[21] show that the magnetoreflection spectra at several photon energies are the same for the three varieties of graphite. The conclusions drawn from that study[21] are that the SWMcC model applies to all three varieties of graphite for the same choice of band parameters.

We now present results on the magnetoreflection spectra in graphite, directed toward the analysis of the H-point resonances. Magnetoreflection traces taken with unpolarized and $\oplus$ and $\ominus$ circularly polarized light are illustrated in Fig. 4. These traces show several H-point resonances, denoted by $m, m^{\pm}$ = integer, with m identified with N in Eqs. (16) and discussed more fully below. It is seen in Fig. 4 that the interpretation of the widely spaced H-point resonances is complicated by the superposition of numerous closely spaced K-point resonances denoted by their (initial, final) Landau-level indices. In order to determine the experimental line shape for the H-point resonances, we have as a first approximation connected the midpoints of the K-point resonances as shown in Fig. 4 and the resonance point has been taken

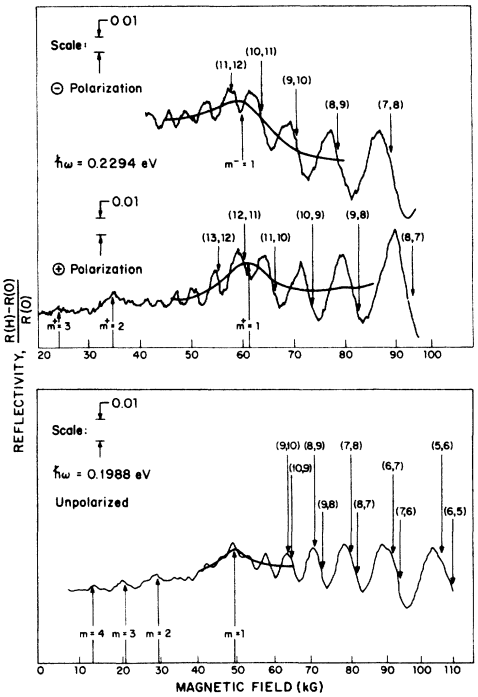

FIG. 4. Magnetoreflection trace on pyrolytic graphite taken at $\hbar\omega = 0.2294$ eV with circularly polarized light (from Ref. 17) and at $\hbar\omega = 0.1988$ eV using unpolarized radiation (from Ref. 20). The K-point transitions are labeled with parentheses indicating (initial, final) levels. The H-point transitions refer to the superposition of two transitions: $E_m^H(-1) \rightarrow E_{m+1}^H(+1)$, $E_{m-1}^H(-2) \rightarrow E_m^H(+2)$ for ⊖ polarization labeled by the integer m^-, and $E_{m+1}^H(-1) \rightarrow E_m^H(+1)$, $E_m^H(-2) \rightarrow E_{m-1}^H(+2)$ for ⊕ polarization labeled by the integer m^+. All four transitions contribute for unpolarized radiation where the H-point resonance is labeled by the integer m. The figure illustrates the construction of an experimental H-point resonance line by connecting the midpoints of the closely spaced K-point structures.

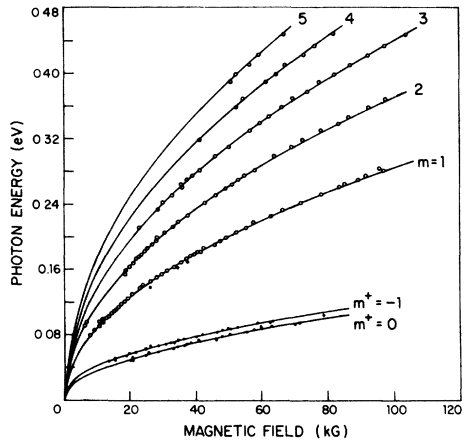

FIG. 5. Summary of H-point resonances covering a wide range of photon energies and magnetic fields. Data from Ref. 13, indicated by open circles, are taken with unpolarized light. Data from Ref. 17 and the present data are taken with circularly polarized light, and are indicated by closed circles. The curves passing through the experimental points represent a least-square fit of these data to Eqs. (16c) and (18).

at the reflectivity maximum. Similar line shapes are observed for H-point resonances with $m \geq 1$, independent of whether the incident light is unpolarized or is ⊕ or ⊖ circularly polarized.

In the original study of H-point transitions,[20] the choice of the resonance point within the magnetoreflection linewidth was arbitrarily taken at the reflectivity maximum. This choice has now been substantiated by a magnetoreflection line-shape calculation for the resonant structures associated with H-point interband transitions.[22] The present study of H-point interband transitions for $m \geq 1$ is in good agreement with the earlier work[13,20] and provides values for the band parameters $|\gamma_0| = 3.16 \pm 0.07$ eV and $|\Delta| = 0.008 \pm 0.004$ eV. The data for H-point resonances are summarized by the points in Fig. 5.

In the present work particular emphasis is given to the two nondegenerate states at the H point denoted by $E_0^H(+1)$ and $E_{-1}^H(+2)$. Transitions to these special states differ from H-point transitions to all the other H-point states (which are doubly degenerate) with respect to polarization dependence, line-shape characteristics, greater sensitivity to the magnitude of Δ, and sensitivity to the sign of Δ, as is discussed below.

The intensity of an H-point magnetoreflection resonance which is identified with the doubly degenerate final states arises from four degenerate contributions: two for ⊖ circular polarization, $E_N^H(-1) \rightarrow E_{N+1}^H(1)$ and $E_{N-1}^H(-2) \rightarrow E_N^H(+2)$; and two for ⊕ circular polarization, $E_{N+1}^H(-1) \rightarrow E_N^H(+1)$ and $E_N^H(-2) \rightarrow E_{N-1}^H(+2)$. Transitions to the two nondegenerate H-point levels occur only for the ⊕ sense of circular polarization, which follows from the discussion in Sec. II. Although the special transitions $E_1^H(-1) \rightarrow E_0^H(+1)$ and $E_0^H(-2) \rightarrow E_{-1}^H(+2)$ are of comparable energy for large magnetic fields, these transitions must be treated as nondegenerate, having an energy difference approaching $|\Delta|$ at low magnetic fields. In Fig. 6 the magnetoreflection traces taken by Schroeder *et al.*[18] to study K-point interband transitions are seen to provide evidence supporting the polarization selection rules for the special H-point transitions. For the upper trace taken with ⊖ circularly polarized radiation, we see that the baseline remains independent of magnetic field, consistent with the absence of H-point transitions, while the lower trace taken with ⊕ circularly polarized radiation shows a characteristic baseline variation, con-

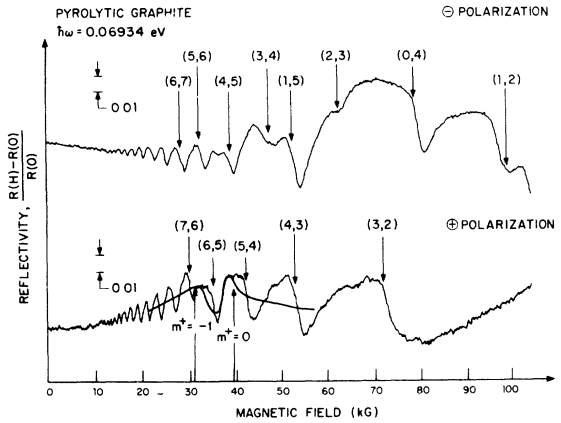

FIG. 6. Magnetoreflection traces in pyrolytic graphite at $\hbar\omega = 0.069\,34$ eV for ⊖ and ⊕ circular polarization (from Ref. 18). At this photon energy, no H-point resonances have been identified in the trace for ⊖ polarization, which shows a number of K-point transitions. From the trace for ⊕ polarization, structures associated with the $m^* = -1$ and $m^* = 0$ transitions at the H point have been identified. The arrows indicating these H-point transitions are drawn using the least-squares-fitting results of Fig. 5.

sistent with the presence of an H-point transition superimposed on the numerous K-point transitions. In accordance with the nondegeneracy of the $E_0^H(+1)$ and $E_{-1}^H(+2)$ levels, the H-point transitions in Fig. 6 are interpreted in terms of two resolved resonant structures, and this is discussed more fully below.

Further insight into the difference between the H-point transitions to degenerate and nondegenerate states can be obtained from consideration of the magnetoreflection resonant line shapes. The simplest case to consider is that to the degenerate levels using monochromatic circularly polarized incident light where the magnetoreflection trace is generated by sweeping the magnetic field (e.g., see traces in Fig. 6). For ⊖ circular polarization, the Landau level diagram of Fig. 3 indicates that the transitions for the ± 1 ladder $E_N(-1) \rightarrow E_{N+1}(+1)$ exhibit a magnetic field *threshold* at the H point ($\xi = \frac{1}{2}$), with transitions occurring at higher magnetic-field values as we move away from the H point. Because of the sharp maximum in the joint density of states at the H point, the maximum contribution to the resonance line occurs for ξ values in the neighborhood of $\xi = \frac{1}{2}$. Figure 3 further shows that for the ± 2 ladder, the transitions $E_{N-1}(-2) \rightarrow E_N(+2)$ exhibit a magnetic field *cutoff* at the H point ($\xi = \frac{1}{2}$), with transitions occurring at lower magnetic fields as we move away from the H point, the maximum contribution again occurring for $\xi \simeq \frac{1}{2}$, because of the singularity in the joint density of states at the H point. This physical picture predicts a magnetoreflection line shape where the contribution from the H point itself (the resonant magnetic-field point) occurs at the reflectivity maximum with tails extending to higher magnetic fields (from the ± 1 ladder contributions) and to lower magnetic fields (from the ± 2 ladder contributions). A similar line shape is predicted for transitions to the doubly degenerate H-point levels under ⊕ circularly polarized radiation. A detailed line-shape calculation based on the SWMcC model[22] confirms this physical picture of the magnetoreflection

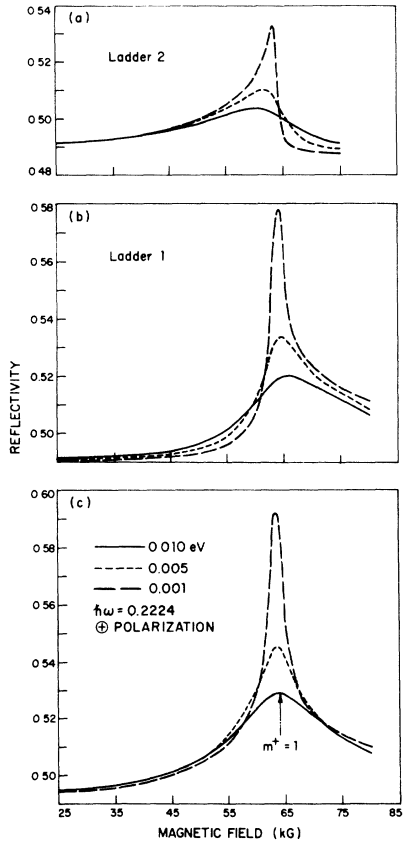

FIG. 7. Results of the H-point magnetoreflection line-shape calculation for transitions to degenerate H-point levels using the SWMcC model. Results are shown for three values of the relaxation time where $\hbar/\tau$ is expressed in units of eV. (a) Contribution from the $E_1(-2) \rightarrow E_0(+2)$ transition to the $m^* = 1$ resonance for ⊕ circular polarization at $\hbar\omega = 0.2224$ eV, illustrating the high-field cutoff. (b) Contribution from the $E_2(-1) \rightarrow E_1(+1)$ transition to the same $m^* = 1$ line under the same conditions, illustrating the low-field threshold. (c) Composite of (a) and (b) to simulate trace which would be observed experimentally for ⊕ polarization. A similar line-shape results from the superposition of the corresponding two contributions for ⊖ polarization, and from the superposition of all four contributions in the case of unpolarized radiation.

resonant line shape, as is shown in Fig. 7 and is discussed further below. Results calculated for the H-point transition $E_1(2) \rightarrow E_0(+2)$ for $\oplus$ circular polarization at $\hbar\omega = 0.2224$ eV are shown in Fig. (7a) for relaxation times given by $\hbar/\tau = 0.001$, 0.005 and 0.01 eV; the longer the relaxation time, the greater is the intensity, and the more pronounced is the high-field cutoff for the resonant transition. The companion transition $E_2(-1) \rightarrow E_1(+1)$ for the same sense of polarization, the same photon energy and the same relaxation times is shown in Fig. 7(b) and here the characteristic low-field threshold is evident. We note that the intensity for the transition $E_2(-1) \rightarrow E_1(+1)$ is greater than that for $E_1(-2) \rightarrow E_0(+2)$ resulting in a slightly asymmetric composite line shape for the observable transition between the degenerate H-point levels, shown in Fig. 7(c). This slight asymmetry is however difficult to observe experimentally because the H-point resonances are observed in a background of numerous K-point resonances.

Because of the similarity between the calculated line shapes for the $m \geq 1$ transitions using $\oplus$ and $\ominus$ circular polarizations, the H-point magnetoreflection line shapes observed with either linearly polarized or unpolarized radiation are similar to that discussed above. Experimental H-point resonances labeled $m^{\pm} = 1$ in the traces of Fig. 4 illustrate the similarity in line shape between resonances for unpolarized and for $\oplus$ and $\ominus$ circularly polarized radiation. In Fig. 4 we use the integer m^{+} to label the two degenerate $\oplus$ polarization transitions $E^H_{m+1}(-1) \rightarrow E^H_m(+1)$ and $E^H_m(-2) \rightarrow E_{m-1}(+2)$ and the integer m^{-} to label the two degenerate $\ominus$ polarization transitions $E^H_m(-1) \rightarrow E^H_{m+1}(+1)$ and $E^H_{m-1}(-2) \rightarrow E^H_m(+2)$. To denote transitions observed with unpolarized light, the $\pm$ superscripts are deleted.

This physical picture can also be applied to the consideration of the line shape for the special H-point transitions to the nondegenerate levels. In discussing these transitions, we will use the notation $m^{+} = 0$ to label the $E^H_1(-1) \rightarrow E^H_0(+1)$ transition and $m^{+} = -1$ to label the $E^H_0(-2) \rightarrow E^H_{-1}(+2)$ transition. These special transitions appear only for the $\oplus$ polarization. It is of interest to note that previous studies in the low-photon energy range have emphasized the $\ominus$ polarization because of the important information on the warping of the Fermi surface provided by the variety of "forbidden" resonant structures that are observed with the $\ominus$ polarization.[18]

Experimentally, the line shapes for transitions to the special nondegenerate H-point levels appear to be significantly more asymmetrical than those for the transitions to the degenerate levels. From Fig. 3 it can be seen that the $m^{+} = -1$ transition exhibits a magnetic-field cutoff corresponding to the transition at the H point itself, with contributions to the resonant structure occurring for *lower* magnetic fields as we move away from the H point. This characteristic line shape also results from a detailed line-shape calculation discussed below. If $\Delta < 0$, in accordance with Fig. 3, contributions to the $m^{+} = 0$ resonance will occur at higher magnetic fields than the resonant transitions associated with $m^{+} = -1$. The shape of the Landau-level contours of Fig. 3 predicts a magnetic-field *threshold* at the H-point for the $m^{+} = 0$ transition, with contributions occurring at *higher* magnetic fields as we move away from $\xi = \frac{1}{2}$. Since Fig. 3 shows that the joint density of states for the $m^{+} = -1$ transition decreases more slowly than that for the $m^{+} = 0$ transition as we move away from the H point, the intensity on the low-field side of the $m^{+} = -1$ transition is expected to fall off relatively slower than the intensity on the high-field side of the $m^{+} = 0$ transition; this prediction is confirmed by the detailed line-shape calculation. On the other hand, if $\Delta > 0$, which is the assumption that has been used in the construction of Landau level contours in previous work,[18] the resonance associated with the $m^{+} = 0$ transition exhibits a singularity at a lower magnetic field than the resonance associated with the $m^{+} = -1$ transition. The arguments given above for the general line shape for each of these transitions apply for either sign of Δ. However, the shape of the $m^{+} = 0$ transition near the reflectivity peak could be somewhat different for the two choices of the sign of Δ, because of the sensitivity of the curvature of the $E_0(+1)$ level near the H point to the sign of this parameter.

To illustrate these features we show in Fig. 8 the results of a line-shape calculation for H-point transitions to the nondegenerate levels using the SWMcC model for the energy levels[7] and the optical matrix elements which enter the expression for the optical conductivity[17]

$$\sigma^{\pm} = -\frac{i\hbar}{2} \sum_{l,l'} \left(\frac{f(\epsilon_l) - f(\epsilon_{l'})}{\epsilon_l - \epsilon_{l'}} \right) \times \frac{|\langle l | (e/m) p^{\pm} | l' \rangle|^2}{\hbar\omega - \epsilon_{l'l} + i\hbar/\tau_{ll'}} \,. \tag{27}$$

In this equation $\epsilon_{l'l}$ is the energy separation $(\epsilon_{l'} - \epsilon_l)$ between states l' and l, where l denotes the set of appropriate quantum numbers to describe a Bloch electron in a magnetic field: band index, Landau-level index, wave vector along the applied magnetic field, and a wave-vector component in the plane perpendicular to the magnetic field. In the case where $l = l'$, the term in Eq. (27) within large parentheses is to be interpreted as

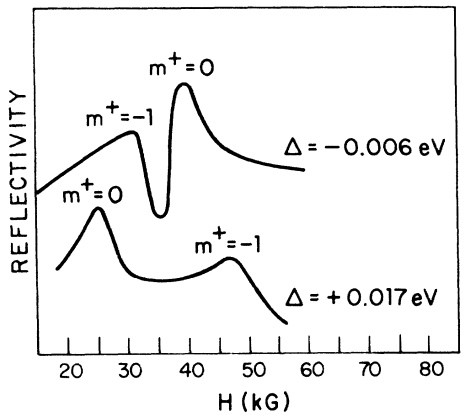

FIG. 8. Results for H-point magnetoreflection line-shape using the SWMcC model for transitions to the two nondegenerate H-point levels at $\hbar\omega = 0.069\,34$ eV (same photon energy as in experimental trace in Fig. 6) and a relaxation time given by $\hbar/\tau = 0.001$ eV. (a) Line shape for the composite $m^+ = -1$, $m^+ = 0$ H-point transitions with $\Delta < 0$. (b) Line shape for the $m^+ = 0$, $m^+ = -1$ transitions with $\Delta > 0$. The actual calculations were made for $\Delta = -0.006$ eV in (a), and $\Delta = +0.017$ eV in (b), which are reasonable choices for Δ in making the identification of P_2 with P_H in (a), and P_1 with P_H in (b). For both the $m^+ = 0$, -1 transitions the resonance point is at the reflectivity maxima.

the derivative of the Fermi function $\partial f(\epsilon_l)/\partial\epsilon_l$. For simplicity, the relaxation time connecting states l and l' is taken as a constant independent of energy, wave vector, or state designations. In this H-point magnetoreflection line-shape calculation we have considered in detail only contributions for $|\xi| \gtrsim 0.45$ to emphasize the H-point structure and to suppress contributions from the K-point transitions. The magnetoreflection line shapes in Fig. 8 are calculated for the same photon energy as in the experimental trace of Fig. 6 with a relaxation time given by $\hbar/\tau = 0.001$ eV, and considering the possibility of either the negative value of $\Delta = -0.006$ eV [Fig. 8(a), corresponding to the identification of the dHvA period P_2 with P_H] or the positive value of $\Delta = +0.017$ eV [Fig. 8(b), corresponding to the identification of P_1 with P_H]. The H-point resonance occurs at the reflectivity maxima in these structures.

If we could extract two well-defined H-point structures for the special nondegenerate transitions from the experimental data, then the separation in magnetic field between the two structures could be interpreted to yield an accurate value for $|\Delta|$ and the line-shape characteristics (see Fig. 8) could be interpreted to yield the sign of Δ. Unfortunately, these H-point structures cannot be sufficiently well resolved experimentally to provide a truly convincing identification by themselves for the sign of Δ.

On the other hand, by correlating the H-point magnetoreflection results with the dHvA results for the minority periods, we are then able to deduce both the magnitude and sign of Δ. For example, for the photon energy $\hbar\omega = 0.0693$ eV (for which the traces in Fig. 6 are taken), the identification of the minority period P_2 with P_H ($\Delta = -0.006$ eV) predicts a resonant field of 31 kG for the $m^+ = -1$ transition and 42 kG for the $m^+ = 0$, while the identification of P_1 with P_H ($\Delta = +0.017$ eV) predicts a resonant field of 25 kG for the $m^+ = 0$ transition and 46 kG for the $m^+ = -1$ transition. The experimental trace in Fig. 6 for $\oplus$ polarization shows an H-point reflectivity maximum at about 31 kG with a line shape generally consistent with that shown in Fig. 8 for the $m^+ = -1$ transition.

The location of a second H-point resonance in Fig. 6 at higher magnetic fields (~ 40 kG) is difficult to identify directly from the experimental trace. Some guidance in this identification is provided by the anomalous line shape in the K-point resonances in the region of the H-point resonances. For example, following the assignment suggested tentatively by the identification with the dHvA minority period P_2, we note that the reflectivity maximum between the (7,6) and (6,5) K-point transitions is anomalously broad, suggesting that the H-point maximum occurs just beyond the (7,6) K-point resonance. Likewise, at higher magnetic fields, the anomalous appearance of the reflectivity maximum between the (6,5) and (5,4) K-point transitions is also consistent with an H-point resonance occurring just below the (5,4) K-point resonance.

Although this argument by itself is somewhat tenuous, some confirmation for these ideas can be derived by considering the relative photon energy dependence of these superimposed H- and K-point resonant line shapes. Because of the larger Landau-level separations at the H point relative to those at the K point, the resonant structures on a given magnetoreflection trace which are identified with the H-point transitions are expected to move to higher fields more rapidly with increasing photon energy than the neighboring K-point resonances. According to this argument, we would expect the anomalous flat-top reflectivity maximum between the (6,5) and (7,6) K-point transitions in Fig. 6 to disappear as we go to higher photon energies and the H-point structure has moved to the position of the (6,5) K-point resonance near the reflectivity minimum. Then at yet higher photon energies we would expect H-point structure to appear in the region between the (6,5) and (5,4) K-point resonances. To make

this argument definite, let us consider the assignment of $\Delta = -0.006$ eV which appears to be roughly consistent with the trace in Fig. 6. Experimentally, we find that at a photon energy of 0.084 eV (data are now shown here) there is no anomalous flat top on the reflectivity maximum between the (7,6) and (6,5) K-point transitions, but instead a similar flat-top anomaly appears in the reflectivity maximum between the (6,5) and (5,4) K-point transitions which can be identified through the $\Delta = -0.006$-eV assignment with the $m^+ = -1$ resonance located at 47 kG; also at $\hbar\omega = 0.084$ eV, there is an anomalous flat-top feature in the reflectivity maximum between the (5,4) and (4,3) K-point resonances, which is consistent with the placement of the $m^+ = 0$ transition at 59 kG. Thus, the magnetoreflection trace at $\hbar\omega = 0.084$ eV is rather similar to that shown in Fig. 6, except that the two anomalous flat-top reflectivity maxima have translated by one K-point quantum number. A change in the appearance of the magnetoreflection trace is found as we go to a slightly higher photon energy, as for example $\hbar\omega = 0.088\,45$ eV [see Fig. 9(a)] where the H-point resonance identified with the $m^+ = -1$ transition has moved over and is very close to the halfway point between the (6,5) and (5,4) K-point transitions. For this particular photon energy, the reflectivity maxima for both the K-point and H-point transitions lie close to each other, thereby giving rise to a well-defined reflectivity maximum, but rising significantly further above the baseline than any of the other reflectivity maxima. At $\hbar\omega = 0.088\,45$ eV, the $m^+ = 0$ transition is expected to be close to the indicated arrow for the $\Delta = -0.006$ eV choice. From Fig. 9(a) this resonance appears to result in a flat-top anomaly in the reflectivity maximum between the (5,4) and (4,3) K-point transitions, somewhat similar in appearance to the situation between the (6,5) and (5,4) K-point resonances in Fig. 6. It is of interest to note that the (4,3) K-point resonance has a reflectivity value close to the baseline reflectivity.

In Fig. 9(b) we see what happens when the photon energy has increased to $\hbar\omega = 0.0966$ eV. Here no flat-top reflectivity anomalies are found, which also turns out to be consistent with the assignment of $\Delta = -0.006$ eV. At this photon energy the resonance for the $m^+ = -1$ H-point transition has moved to 63 kG which lies about 2.5 kG above the (5,4) K-point resonance and appears as a well-resolved peak; the reflectivity structure peaking at 63 kG does not fit into the picture for any of the K-point resonances. The assignment of $\Delta = -0.006$ eV locates the $m^+ = 0$ H-point resonance at 77 kG, which lies very close to the reflectivity minimum associated with the (4,3)

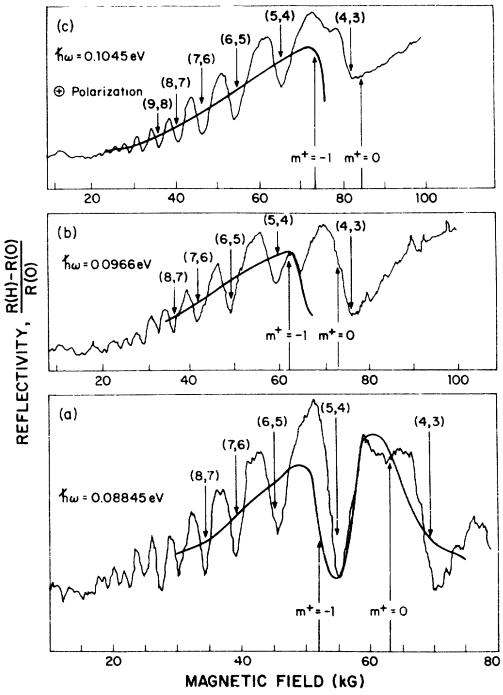

FIG. 9. Magnetoreflection traces taken at various photon energies with ⊕ circular polarization (a) $\hbar\omega = 0.088\,45$ eV, (b) $\hbar\omega = 0.0966$ eV, (c) $\hbar\omega = 0.1045$ eV. Comparison of the traces indicate that as the photon energy increases the H-point resonances move more rapidly to higher magnetic fields than do the K-point resonances. Changes in the line shape of the superimposed H- and K-point resonances are utilized in analyzing the H-point spectra. The arrows for the H-point resonances are drawn using the least-square-fitting analysis of Fig. 5.

K-point resonance. The only evidence for the $m^+ = 0$ transition is the high value for the reflectivity at the (4,3) K-point resonance which is well above the baseline, in contrast with the appearance of this resonance at other photon energies [see Figs. 6 and 9(a)].

At the photon energy of $\hbar\omega = 0.1045$ eV shown in Fig. 9(c), the location of the $m^+ = -1$ transition is predicted to be at 75 kG and appears as an additional structure superimposed on the (4,3) K-point structure as indicated in the figure. The H-point $m^+ = 0$ transition is predicted to be at 90 kG at this photon energy and is not discernible in this figure except for the anomalously high baseline reflectivity at the high-field end of this trace. As we move to yet higher photon energies, the reflectivity maximum between the (5,4) and (4,3) K-point transitions sharpens up as the $m^+ = -1$ H-point resonance moves into coincidence with the (4,3) K-point transition.

The consistency between the observed H-point

structures and the predictions of the $\Delta = -0.006$-eV assignment provides strong evidence in support of the identification of the $P_2 = 3.03 \times 10^{-4}$ G^{-1} with P_H in Eq. (1). If, on the other hand, the $P_1 = 1.35 \times 10^{-4}$ G^{-1} is identified with P_H, then the locations of the $m^* = 0$ resonance are predicted to be at 25 kG in Fig. 6, at 53 kG in Fig. 9(a), at 56 kG in Fig. 9(b) and at 60 kG in Fig. 9(c); likewise, the locations of the $m^* = -1$ resonances for this second assignment would be at 45 kG in Fig. 6, at 67.3 kG in Fig. 9(a), at 83 kG in Fig. 9(b), and at 96 kG in Fig. 9(c). Because of the broadening of the H-point resonances lines due to relaxation processes, there is a small shift between the reflectivity maxima and the H-point resonance fields. These shifts can be predicted from our H-point magnetoreflection line-shape calculation and do not amount to more than 2 or 3 kG in the case of maximum shift. From this discussion, it is clear that the experimental observations for the H-point transitions are not in good agreement with the predictions resulting from the choice of $\Delta = +0.017$ eV.

To obtain an independent determination of Δ, magnetoreflection traces in the photon energy range $0.0670 < \hbar\omega < 0.1045$ eV have been analyzed to yield resonant magnetic fields for the $m^* = 0$ and $m^* = -1$ H-point transitions. The resonances obtained in this way are summarized in Fig. 5 as the solid circles, and a least-squares fit to these data using Eq. (26) and $\gamma_0 = 3.16$ eV yields a value of $\Delta = -0.008 \pm 0.004$ eV indicated by the solid curves. It has not been possible to identify both the $m^* = 0$ and $m^* = -1$ transitions in all the experimental magnetoreflection traces. In those traces shown in Figs. 6 and 9 where such an identification could not be made, the predicted resonance point is denoted by an arrow. Analysis of these H-point transitions is inconsistent with an assignment of $|\Delta| > 0.012$ eV.

IV. DISCUSSION

An analysis of H-point magnetoreflection data in conjunction with the results for the dHvA minority periods provides strong evidence that the SWMcC band parameter Δ has a negative sign and a value close to -0.006 eV, with the magnetoreflection results yielding $\Delta = -0.008 \pm 0.004$ eV. This study leads to an identification for the minority period $P_2 = 3.03 \times 10^{-4}$ with P_H, the circular orbit about the H point for the magnetic-field orientation $\vec{H} \parallel \vec{c}$.

There is also other evidence in support of the identification of the minority period P_2 with P_H. The anisotropy of the minority period P_2 as the magnetic field is rotated from $\vec{H} \parallel \vec{c}$ ($\theta = 0°$) to $\vec{H} \perp \vec{c}$ ($\theta = 90°$) has been measured by Williamson *et al.*[2] and is found to be $P_2(0°)/P_2(90°) \simeq 2$, taking into account their error in the magnetic-field calibration.[8] The corresponding anisotropy of the period P_H can be estimated by approximating the H-point minority Fermi surface in Fig. 1 by an ellipsoid with the semimajor axis wave vector parallel to the $\vec{c}$ direction given by

$$k_{F,\parallel} \simeq (1/\gamma_1 c_0)\,|(E_F - \Delta)|\,, \tag{28}$$

and with the semimajor axis wave vector perpendicular to the $\vec{c}$ direction given by

$$k_{F,\perp} = (2/\sqrt{3})\,(1/\gamma_0 a_0)[E_F(E_F - \Delta)]^{1/2}\,, \tag{29}$$

so that

$$\frac{P_H(0°)}{P_H(90°)} \simeq \frac{k_{F,\perp}}{k_{F,\parallel}} \simeq \frac{\sqrt{3}}{2}\left(\frac{\gamma_0}{\gamma_1}\right)\left(\frac{a_0}{c_0}\right)\left(\frac{E_F - \Delta}{E_F}\right)^{1/2}. \tag{30}$$

This ratio has a value of 2.1, assuming values for the various parameters of $\gamma_0 = 3.16$ eV, $\gamma_1 = 0.39$ eV, $a_0 = 2.46$ Å, $c_0 = 6.74$ Å, $E_F = -0.026$ eV, and $\Delta = -0.008$ eV. The agreement between this estimate for the anisotropy of P_H and the anisotropy measurements on P_2 is satisfactory, in view of the uncertainty in the experimental data and the approximations made in the calculation. On the other hand, the measurement of the anisotropy ratio for the minority period P_1 yields a value[6] of ~13, which is too large to be consistent with the anisotropy of P_H for any reasonable choice of Δ. This difficulty with the anisotropy of P_1 has also been discussed by Spain.[12]

Because of their small effective masses, the high-mobility minority carriers are believed to contribute significantly to the Hall effect.[12] Estimates of 3×10^{15}/cm^3 to 8×10^{15}/cm^3 have been made[23,24] for the concentration of these minority carriers at 77 K. The volume for an H-point pocket is approximately given by

$$V_H \simeq \frac{4\pi}{3}\left|\frac{E_F(E_F - \Delta)^2}{\gamma_0^2 \gamma_1 a_0^2 c_0}\right|\,; \tag{31}$$

thus a minority-carrier concentration of 5×10^{15}/cm^3 is obtained for the choice $\Delta = -0.006$ eV, and 21×10^{15}/cm^3 for the choice $\Delta = +0.017$ eV. Therefore, the Hall-effect data also support the identification of P_2 with P_H.

Since the H-point minority-carrier pocket volume V_H does not depend strongly on band parameters as associated with interplanar interactions for $|\Delta/E_F| \ll 1$, V_H would not be expected to exhibit a large pressure dependence. From analysis of the pressure dependence of the Hall data, a small pressure dependence of ~1%/kbar is found for the minority-carrier concentration which contributes

to the Hall effect.[25] In contrast, the pressure dependence found experimentally for P_1 is large, indicating a 6% variation in extremal area per kbar.[5] Thus, the results for the pressure dependence of the Hall constant is consistent with the identification of P_2 with P_H. Further discussion of the pressure dependence of the electronic structure and of the various extremal cross-sectional areas is found in a recent publication by Dillon, Spain, and McClure.[26]

Further evidence for the identification of P_2 with P_H comes from a recent analysis of data on the diamagnetic susceptibility χ by Sharma, Johnson, and McClure.[14] Their analysis indicates that a value of $\Delta = -0.010 \pm 0.002$ eV is required to yield satisfactory agreement between the susceptibility data and K-point magnetoreflection data.[18] These authors find that a value of at least 0.35 eV is required for γ_3 to obtain a fit to χ for $\Delta = +0.004$ eV, as proposed by Woollam[6] in identifying P_1 with P_H. Such a large value for γ_3 disagrees with γ_3 values found from cyclotron resonance[27,28] and K-point magnetoreflection studies.[18]

It has been suggested that a second minority period around the H point might arise from the spin-orbit splitting indicated in Fig. 1. However, the magnitude of the spin-orbit splitting is not large enough[11] to give rise to an H-point minority period corresponding to P_1, as has been pointed out by various authors.[12] Soule[1] originally suggested that P_1 might be associated with "outrigger" pieces of Fermi surface. Spain[12] later suggested that because of the trigonal warping of the Fermi surfaces, P_1 may originate through the formation of a carrier pocket in the region of the legs connecting the electron and hole Fermi surfaces. It is also possible that the period P_1 might be identified with the creation and annihilation of special Landau levels[29] which are introduced at the K point by the trigonal warping of the Fermi surface.

Eberhard, Vegas, and Briggs[30] have suggested a totally different identification of the period P_1 based on studies of the angular dependence of P_1. In particular, they have shown that the relation

$$2f_1 = f_e - f_h \tag{32}$$

is well satisfied as the magnetic field is rotated from $\vec{H} \parallel \vec{c}$ to $\vec{H} \perp \vec{c}$. In Eq. (32) the dHvA frequencies f_1, f_e, and f_h, respectively, correspond to the minority period P_1 and the majority electron and hole periods, P_e and P_h. Thus these authors identify P_1 with a beating effect between the majority electron and hole periods. In a somewhat similar vein, Nakao has suggested[31] that the dHvA period P_1 may be associated with magnetic breakthrough effects between minority and majority hole orbits near the H point. Such magnetic breakthrough phenomena could arise through a γ_3-induced mixing of the magnetic energy levels of the E_3 bands when they cross the magnetic energy levels of the E_1 and E_2 bands near the H point.

ACKNOWLEDGMENTS

The authors are thankful to Professor J. W. McClure and Dr. K. Nakao for helpful discussions and to Dr. A. W. Moore for kindly supplying us with the pyrolytic graphite used in the present magnetoreflection measurements.

---

*Work sponsored by the NSF Grant No. LMR 76-12226 and by the Department of the Air Force.

†Visiting scientists, Francis Bitter National Magnet Laboratory, Massachusetts Institute of Technology, Cambridge, Mass.

‡Supported by the NSF.

[1]D. E. Soule, IBM J. Res. Dev. 8, 268 (1964).

[2]S. J. Williamson, S. Foner, and M. S. Dresselhaus, Phys. Rev. 140, A1429 (1965).

[3]S. J. Williamson (unpublished).

[4]D. J. Flood, Phys. Lett. A 30, 178 (1969).

[5]J. R. Anderson, W. J. O'Sullivan, J. E. Schirber, and D. E. Soule, Phys. Rev. 164, 1038 (1967).

[6]J. A. Woollam, Phys. Rev. B 4, 3393 (1971).

[7]J. W. McClure, *Proceedings of the International Conference on the Physics of Semimetals and Narrow Gap Semiconductors, Dallas, Texas*, 1970, edited by D. L. Carter and R. T. Bate (Pergamon, New York, 1971), p. 127.

[8]A correction to the value of $P_2 = 2.24 \times 10^{-4}$ G^{-1} reported in Ref. 2 due to an error in a magnet calibration is given in Refs. 6 and 7.

[9]J. A. Woollam, Phys. Lett. A 32, 115 (1970).

[10]G. Dresselhaus and M. S. Dresselhaus, Phys. Rev. 140, A401 (1965).

[11]J. W. McClure and Y. Yafet, *Proceedings of the Fifth Conference on Carbon* (Pergamon, Oxford and New York, 1960), p. 22.

[12]I. L. Spain, in *Chemistry and Physics of Carbon*, Vol. 8, edited by P. L. Walker and P. A. Thrower (Marcel Dekker, New York, 1973), p. 1.

[13]J. G. Mavroides and M. S. Dresselhaus, Bull. Am. Phys. Soc. 10, 109 (1965).

[14]M. P. Sharma, L. G. Johnson, and J. W. McClure, Phys. Rev. B 9, 2467 (1974).

[15]J. W. McClure, Phys. Rev. 119, 606 (1960).

[16]M. Inoue, J. Phys. Soc. Jpn. 17, 808 (1962).

[17]P. R. Schroeder, Ph.D. thesis (MIT, 1969) (unpublished).

[18]P. R. Schroeder, M. S. Dresselhaus, and A. Javan, *Proceedings of the International Conference on the Physics of Semimetals and Narrow Gap Semiconduc-*

tors, Dallas, Texas, 1970, edited by D. L. Carter and R. T. Bate (Pergamon, New York, 1971), p. 139.
[19]P. R. Schroeder, M. S. Dresselhaus, and A. Javan, Phys. Rev. Lett. 20, 1292 (1968).
[20]M. S. Dresselhaus and J. G. Mavroides, IBM J. Res. Dev. 8, 262 (1964).
[21]W. W. Toy, C. R. Hewes, and M. S. Dresselhaus, Eleventh Biennial Conference on Carbon, Gatlinburg, Tenn. 1973 (unpublished), p. 1; Carbon 11, 575 (1973).
[22]W. W. Toy, M. S. thesis (MIT, 1973) (unpublished).
[23]J. W. McClure, Phys. Rev. 112, 715 (1958).
[24]D. E. Soule, Phys. Rev. 112, 698 (1958).
[25]I. L. Spain, *Proceedings of the Conference on the Electronic Density of States, 1969*, Natl. Bur. Stds. Publ. (U. S. GPO, Washington, D. C., 1969), p. 717.
[26]R. O. Dillon, I. L. Spain, and J. W. McClure (unpublished).
[27]H. Suematsu and S. Tanuma, J. Phys. Soc. Jpn. 33, 1619 (1972).
[28]H. Ushio, T. Uda, and Y. Uemura, J. Phys. Soc. Jpn. 33, 1551 (1972).
[29]G. Dresselhaus, Phys. Rev. B 10, 3602 (1974).
[30]A. Eberhard, J. Vagas, and A. Briggs, Phys. Lett. A 53, 297 (1975).
[31]K. Nakao, J. Phys. Soc. Jpn. 40, 761 (1976).

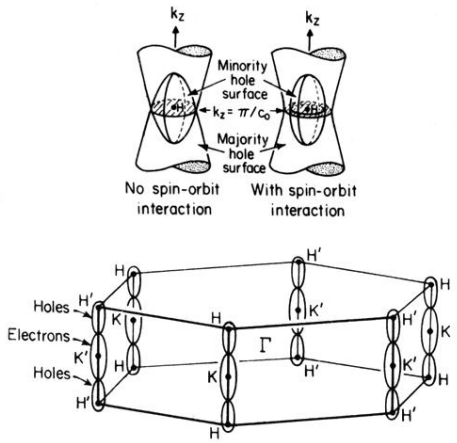

FIG. 1. Fermi surface for minority hole pocket near the Brillouin-zone corner (the *H* point) shown in the extended-zone scheme. This pocket is formed by the overlap of the portions of the Fermi surface which extend beyond the Brillouin-zone boundary and is illustrated for no-spin-orbit interaction, and including spin-orbit interaction. The extremal cross section around the *H* point and perpendicular to the *c* axis is indicated. Bottom: Hexagonal Brillouin zone for graphite showing schematically the locations of the hole and electron Fermi surfaces. Of particular interest are the portions of the hole surface which project beyond the Brillouin-zone boundary and give rise to the minority surface shown in the top figure.